SAND2016-9951C

A Method to Assess Flux Hazards at CSP Plants to Reduce Avian Mortality

Clifford K. Ho,[1, a)] Timothy Wendelin,[2] Luke Horstman,[1] and Julius E. Yellowhair[1]

[1]*Sandia National Laboratories, P.O. Box 5800, MS-1127, Albuquerque, NM 87185-1127, USA*
[2]*National Renewable Energy Laboratory, Golden, CO 80401*

[a)]*Corresponding author: ckho@sandia.gov*

Abstract. A method to evaluate avian flux hazards at concentrating solar power plants (CSP) has been developed. A heat-transfer model has been coupled to simulations of the irradiance in the airspace above a CSP plant to determine the feather temperature along prescribed bird flight paths. Probabilistic modeling results show that the irradiance and assumed feather properties (thickness, absorptance, heat capacity) have the most significant impact on the simulated feather temperature, which can increase rapidly (hundreds of degrees Celsius in seconds) depending on the parameter values. The avian flux hazard model is being combined with a plant performance model to identify alternative heliostat standby aiming strategies that minimize both avian flux hazards and negative impacts on plant performance.

INTRODUCTION

Avian mortality at concentrating solar power (CSP) plants has received a significant amount of attention in recent years [1-4]. Studies at Solar One [5] and at the Ivanpah Solar Electric Generating System in California [6] have indicated that birds can be singed when flying through regions of high solar irradiance (flux) created by reflections from thousands of heliostats. Ho [2] summarized previous studies indicating that the high-flux regions likely to cause avian mortality are from standby heliostats, which reflect the sunlight to a location next to (but not on) the receiver (**FIGURE 1**). The air in these regions is typically transparent to radiation, so the air is not hot. However, when birds fly through these high-flux regions, their temperatures can increase rapidly and cause singeing.

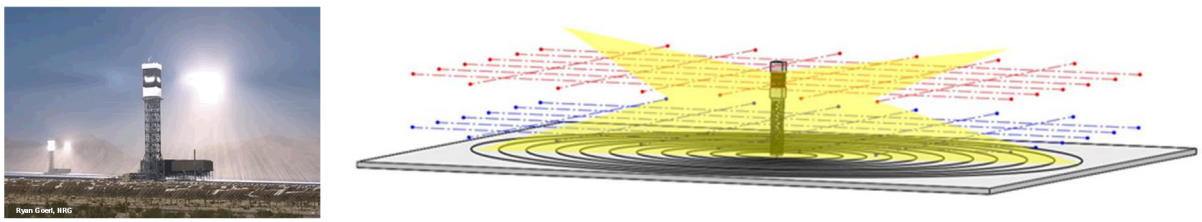

FIGURE 1. Left: Illumination of standby heliostat aim points next to the receiver at Ivanpah. Right: Grid of prescribed bird flight paths in the irradiated region that are used to assess potential avian flux hazards in this study.

During the first year of operation at Ivanpah, a direct-steam 390 MW_e CSP plant with three power towers, H.T. Harvey & Associates reported 703 bird fatalities from 2013 – 2014, of which 45% were caused by singeing [1]. Adjusting the number of fatalities for search efficiency and carcass removal from wildlife, H.T. Harvey & Associates estimated that the total avian mortality for the first year was 1492 (42.6%) of birds of known causes and 2012 (57.4%) of birds from unknown causes. Of the bird deaths due to known causes, 47.4% were singed, and 51.9% died of collision effects, and 0.7% died from other causes. More recent results from 2014 – 2015 showed

that there were an estimated 2500 bird fatalities from known causes and 3686 fatalities from unknown causes. Of the known fatalities, 45% were from singeing, and 54% were from collision. Accounting for variability in the presence of non-resident birds (fall migration), "fatality estimates for the first year and second year differ only slightly" [6]. Since then, Ivanpah has implemented bird deterrents (acoustic, visual, tactile, and chemosensory) that are being evaluated.

During preliminary tests at Crescent Dunes, a 110 MW_e molten-salt power-tower plant in Tonopah, Nevada, thousands of heliostats were aimed at standby points above the receiver, resulting in reported bird deaths as the birds flew through the concentrated flux [7]. SolarReserve decided to spread the standby aim points over several hundred meters to reduce the peak flux. Stantec Consulting Services, which was hired to perform monthly avian mortality surveys at Crescent Dunes, reported only 54 subsequent bird deaths in 2015 throughout the facility, including a 3 km radius outside the facility boundary [8].

This paper introduces a method to assess avian flux hazards at CSP plants. Our goal is to determine alternative heliostat standby aiming strategies that minimize avian mortality caused by solar flux while reducing impacts on the plant's operational performance.

APPROACH

The general approach to identifying alternative heliostat standby aiming strategies that minimize impacts on avian mortality and operation performance is summarized as follows:

- Avian Flux Hazard Evaluation
  - Develop a heat transfer model that determines the bird feather temperature as a function of irradiance and other relevant parameters
  - Develop a solar flux model to estimate irradiance as a function of location in the airspace above a CSP plant for alternative heliostat aiming strategies
  - Use the heat transfer model and solar flux model to determine the bird feather temperature along prescribed transects in the airspace above the CSP plant
  - Record the total number of minutes that the bird feather temperature exceeds the safe threshold for each aiming strategy and identify options that minimize the time of exceedance
- Operational performance evaluation
  - For each alternative heliostat standby aiming strategy, determine the maximum time required for the reflected light from the heliostats to move from the standby aim point to the receiver (slew time)
  - Use the ratio of the slew time for alternative standby aiming strategies to that of a baseline aiming strategy to obtain a slew-time ratio (multiplier)
  - Determine the baseline start-up time for the CSP plant
  - Take the product of the slew-time ratio and the start-up time for the baseline case to estimate the impact of additional slew time (if any) on energy production via an increase in start-up time
  - Estimate the annual energy production using System Advisor Model [9] for the different standby aiming strategies and slew times to identify options that minimize impact on energy production

The remainder of this paper focuses on the avian flux hazard evaluation. Ongoing efforts to evaluate the impact of alternative heliostat aiming strategies on plant operational performance will be presented in a future paper.

Modeling Bird Feather Temperature

FIGURE 2 shows a schematic of a bird feather, which consists of barbs emanating from a main shaft (rachis). Each barb consists of a smaller shaft (ramus) that has two rows of barbules on either side that interconnect with hooks (pennulae) to adjacent barbules. The feather material is composed predominantly of keratin, which can undergo structural changes when heated [10, 11]. Studies have shown that at about 160 °C, bonds in the molecular structure are broken, which can permanently weaken the feather [10, 12].

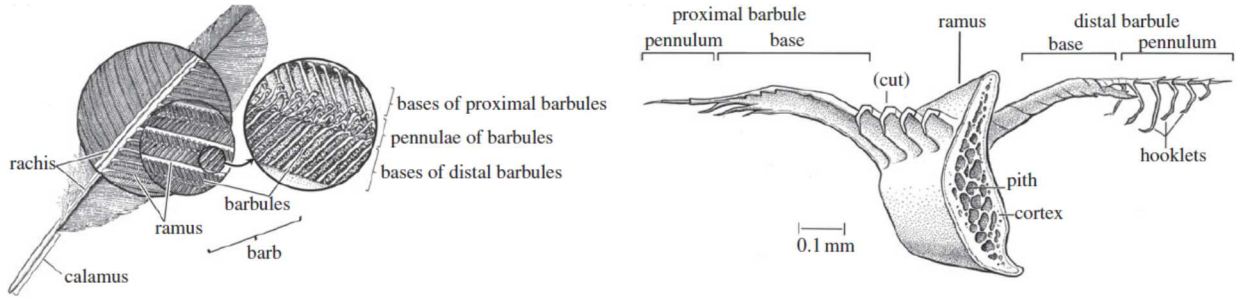

FIGURE 2. Feather morphology. [13]

FIGURE 3 depicts a feather experiencing solar irradiance, thermal radiation, and convection. Heat transfer occurs on one side only (the side exposed to solar irradiance) since the other side of the feather is assumed to be adiabatic (insulated by other feathers). The area, A_s, exposed to solar irradiance, thermal emittance (re-radiation), and convection is assumed to be equal.

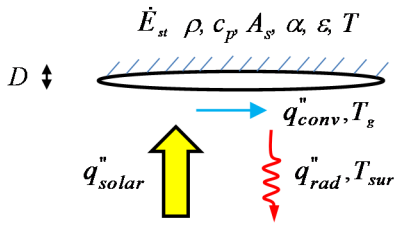

FIGURE 3. Energy balance on control volume of feather barb exposed to solar irradiance.

Neglecting temperature gradients in the feather,* an energy balance on the feather yields the following expressions:

$$\dot{E}_{st} = \dot{E}_{in} - \dot{E}_{out} \tag{1}$$

$$\left(\rho c_p\right)\left(A_s D\right)\frac{dT}{dt} = \alpha q''_{solar} A_s - q''_{conv} A_s - q''_{rad} A_s \tag{2}$$

or

$$\rho c_p D\frac{dT}{dt} = \alpha q''_{solar} - h\left(T - T_g\right) - \varepsilon\sigma\left(T^4 - T_{sur}^4\right) \tag{3}$$

Where

$\dot{E}_{st}$ = Rate of energy stored in feather (W)
$\dot{E}_{in}$ = Rate of energy entering feather (W)
$\dot{E}_{out}$ = Rate of energy leaving feather (W)
q''_{solar} = Solar irradiance (W/m^2)
q''_{conv} = Convective heat flux (W/m^2)
q''_{rad} = Thermal emissive flux (W/m^2)
A_s = Surface area of feather exposed to irradiance (m^2)
ρ = Feather density (kg/m^3)
c_p = Feather specific heat (J/kg-K)

* The Biot number (ratio of internal conductive resistance to radiative and convective resistances) is calculated to be 0.1, indicatingthat the feather can be assumed isothermal and a lumped capacitance model is valid. The average radiative resistance is calculatedassuming a feather temperature of 160 °C and a surrounding temperature of 25 °C, yielding an effective radiative heat transfer coefficient of ~11 W/m^2-K. The convective heat transfer coefficient is calculated to be ~28 W/m^2-K based on a flight speed of 8 m/s.

D = Thickness of feather (m)
t = Time (s)
T = Temperature (K)
T_g = Ambient gas temperature for convective heat loss (K)
T_{sur} = Surrounding temperature for radiative heat loss (K)
V = Feather volume (m^3) = A x D
α = Solar absorptance of feather (-)
ε = Thermal emittance of feather (-)
σ = Stefan-Boltzmann constant (5.67e-8 W/m^2-K^4)

Integrating Eq. (3) yields the following expression:

$$\int_{T_i}^{T_{i+1}} \rho D c_p dT = \int_{t_i}^{t_{i+1}} \left(\alpha q''_{solar} - h\left(T_i - T_g\right) - \varepsilon\sigma\left(T_i^4 - T_{sur}^4\right)\right) dt \tag{4}$$

or

$$T_{i+1} = T_i + \frac{1}{\rho D c_p}\left(\alpha q''_{solar} - h\left(T_i - T_g\right) - \varepsilon\sigma\left(T_i^4 - T_{sur}^4\right)\right)\Delta t \tag{5}$$

Where i is the time step and Eq. (5) is solved by marching forward in time where $\Delta t = t_{i+1} - t_i$. The thermal properties of air (kinematic viscosity, thermal conductivity, Prandtl number) are a function of the film temperature (average of air temperature and feather temperature) and change as the feather temperature changes. Polynomial functions for these thermal properties were derived from data from [14]. The heat transfer coefficient, h, was determined from the Nusselt number, which was calculated based on the Blasius solution for steady, incompressible, laminar air flow over the feather:

$$Nu = \frac{hL}{k_{air}} = 0.664\,\mathrm{Re}_L^{1/2}\,\mathrm{Pr}^{1/3} \tag{6}$$

where

$$\mathrm{Re}_L = \frac{uL}{\nu} \tag{7}$$

and L is the characteristic length (m) of the feather parallel to air flow, k_{air} is the thermal conductivity of air (W/m-K), Pr is the Prandtl number (ratio of momentum and thermal diffusion), u is the air velocity over the feather (m/s), and ν is the kinematic viscosity of air (m^2/s). **TABLE 1** shows the parameter values that are used in this study and associated references. The solar absorptance and thermal emittance of the feather are assumed to be equal, and they account for the radiative view factor for solar irradiance on the feather and thermal emission to the environment.

TABLE 1. Summary of input parameters used in the analytical model..

Parameter	Baseline Value	Min	Max	Reference / Comments
Thickness of feather* (m), D	1.00E-04	1.00E-05	6.00E-04	Based on thickness of barbule [12, 13, 15]
Characteristic length of feather (m), L	0.15	0.0762	0.3048	Lower bound assumed to be 50% of baseline length of 6 inches (0.15 m) [12]; upper bound assumed to be twice the baseline length
Heat capacity of feather (ρ*c_p) (J/m^3-K)	2.0E+06	9.95E+05	1.99E+06	Lower bound based on half of keratin density due to void space [12]; upper bound used keratin density and reported specific heat
Air velocity over feather (m/s), u	8.05	4.02	16.09	Lower bound assumed to be 50% of assumed baseline velocity of 8 m/s; upper bound assumed to be twice the baseline velocity
Thermal conductivity of feather (W/m-K), k_{air}	0.04	N/A	N/A	Used to determine heat transfer coefficient from calculated Nusselt number [16, 17]

Parameter	Baseline Value	Min	Max	Reference / Comments
Heat transfer coefficient (W/m^2), h	28	calculated	calculated	Calculated from air velocity and thermal properties
Surround temperature for convection and radiation (K), T_{sur}	298	273	313	Lower bound assumed to be 0 C; upper bound assumed to be 45 C based on upper limit used by [12]
Effective feather absorptance or emittance, α or ε	1	0.2	1	Lower bound assumes a white feather (~0.4 absorptance) with a 0.5 view factor; upper bound assumes black feather
Initial feather temperature (K)	298	298	433	Lower bound assumed to be 25 C (in between lower limit for surround temperature and body temperature of 40 C; upper limit assumed to be hazard limit of 160 C
Irradiance (W/m^2), Q	N/A	1000	1.00E+06	Lower bound is one sun; assume upper bound is 1000 suns

*The diameter of individual barbules has been reported to be ~2– 6 microns for goose feathers, and the thickness of the ramus holding the barbules has been reported to be ~70 microns in ospreys [15]. For the purposes of this heat-transfer analysis, we assume the baseline thickness of the barb to be ~100 microns, as shown in FIGURE 2.

Solar Flux Modeling

SolTrace and SolarPILOT [18] were used to generate flux maps for the NRG-operated Ivanpah Unit 2 power tower. The solar field of Unit 2 consists of 60,127 heliostats. Each heliostat consists of two panels, each panel being 2.3 meters wide and 3.3 meters high. Each heliostat, depending on its location in the field has one of four focal lengths7: 250, 450, 700 or 1000 meters. For purposes of this study, each heliostat was modeled as one mirror 4.6 meters wide and 2.3 meters high with the appropriate focal length for its location. Typical optical errors for such heliostats were assumed in the model. Heliostat layout data were provided by NRG. The Unit 2 receiver is 17 meters on a side and 22 meters tall. The vertical midpoint of the receiver is 122 meters from the ground. For each of four representative days of the year (Spring equinox (March 20), Summer solstice (June 21), Fall equinox (September 23) and Winter solstice (December 21)) and two representative times of the day (solar noon and three hours before solar noon), planar horizontal flux maps spanning the full area of the heliostat field are being generated at elevations of 60, 122 and 150 meters for a baseline stand-by aiming configuration and three alternative stand-by aiming configurations. The baseline aim-point strategy is shown schematically in **FIGURE 4**. For the baseline case, each heliostat is aimed tangentially in a clockwise fashion to an imaginary circle surrounding the receiver at a height above the ground equal to the receiver midpoint height of 122 meters. The radius of this circle is 25 meters. Three alternative aiming strategies will also be analyzed. The first is similar to the baseline in that heliostats are still aimed clockwise about the receiver, but instead of tangential to a circle at the receiver midpoint height, aim-points are randomly spread across an annular region between 25 meters and 60 meters radially from receiver midpoint height. The second and third alternatives are similar to the first except that heliostat aiming is also randomized between the clockwise and counter clockwise directions and both a 25 to 60 meter radial annulus and a 25 to 250 meter radius annulus are investigated. These are illustrated in Figure 4.

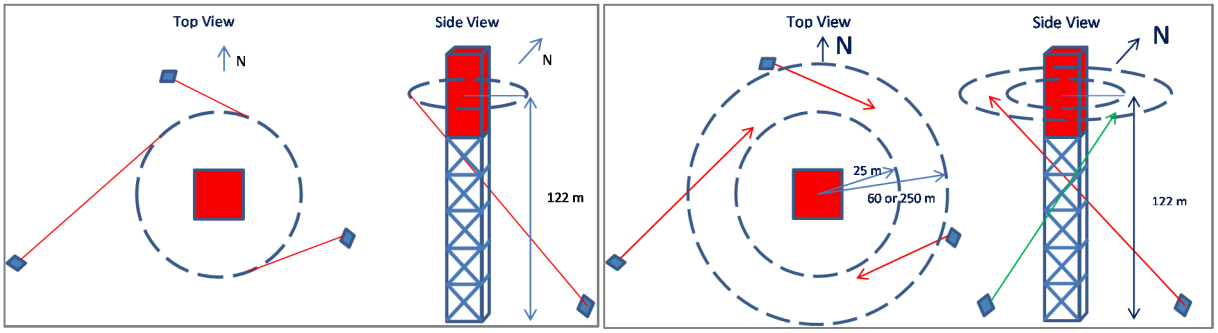

FIGURE 4. Baseline heliostat standby aiming strategy (left). Alternative standby aiming strategies (right). Alternative #1 shown in red, alternatives #2 and #3 shown in green for a 60 and 250 meter outer radius annulus respectively.

RESULTS

Analysis of Bird Feather Temperature with Constant Irradiance

FIGURE 5 shows the predicted feather temperature as a function of time for the baseline case with different (but constant) solar irradiances using Eq. (5) with a time step of 0.1 seconds. The value of 1 kW/m^2 represents the irradiance from one sun (the irradiance a bird would receive from the sun on a clear day), while values of 4 kW/m^2 and 50 kW/m^2 represent solar concentrations of 4 suns and 50 suns, respectively, induced by the heliostat field. The temperatures increase to a steady-state equilibrium temperature at which the heat gain from the solar irradiance equals the heat loss from thermal radiation and convection. The steady-state temperature can be determined by setting the left-hand side of Eq. (3) equal to zero and solving for the feather temperature. The steady-state feather temperatures with solar irradiances of 1, 4, and 50 suns are 54 °C, 130 °C, and 610 °C, respectively, and are reached within 10 – 30 seconds of exposure.

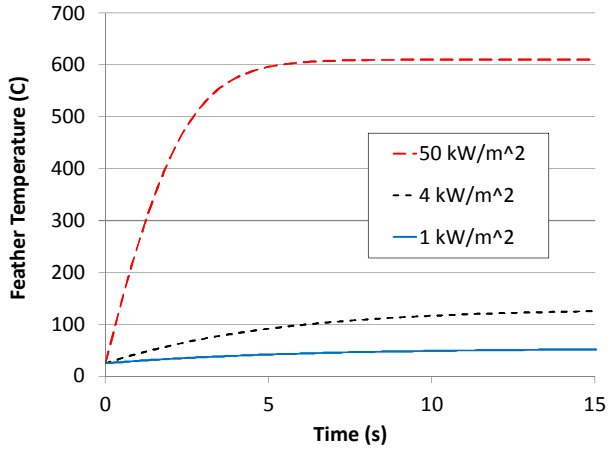

FIGURE 5. Feather temperature as a function of time using different solar irradiances and baseline input values.

Probabilistic simulations were performed to determine the most important input parameters that impact the modeled temperature rise of the feather. **TABLE 1** shows the input parameters and their uncertainty distributions that were considered in the model. Values were sampled from each of the eight uncertain input parameters using up to 3000 realizations to determine the distribution of temperature rise (in 0.01 seconds) (see **FIGURE 6**). Results show that the feather temperature rise can vary significantly, from less than 1 °C to over 1000 °C. A stepwise rank regression analysis was performed which showed that the most important parameters impacting the modeled temperature rise were the irradiance (positive correlation), feather thickness (negative correlation), absorptance (positive correlation), and feather heat capacity (negative correlation).

Bird Feather Temperature Along a Flight Path with Variable Irradiance

FIGURE 7 shows the simulated bird feather temperature along a flight path 60 m above the ground (halfway between the ground and the receiver midpoint) and the associated irradiance distribution using baseline parameter values and the baseline heliostat standby aiming strategy. Results show that the feather temperature increases as the irradiance increases, but the feather temperature can also decrease if the irradiance is less than the convective and radiative heat losses. In this example, the bird feather temperature remains below the safe threshold of 160 °C (433 K). Future work will evaluate the bird feather temperature for numerous flight paths (**FIGURE 1**), alternative aiming strategies, and different dates and times of the day as detailed in the approach section. The operational performance of the plant will also be evaluated using the heliostat slew times, and alternative aiming strategies that minimize both avian flux hazards and slew times will be identified.

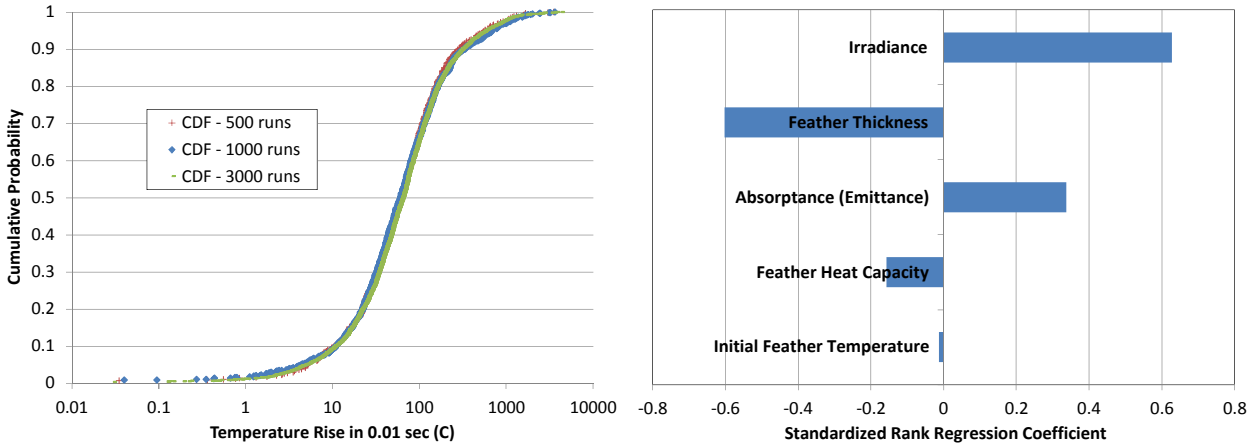

FIGURE 6. Left: Cumulative distribution function of stochastic temperature rise for different numbers of realizations. Right: Stepwise standardized rank-regression coefficients of most important input parameters that impact temperature rise.

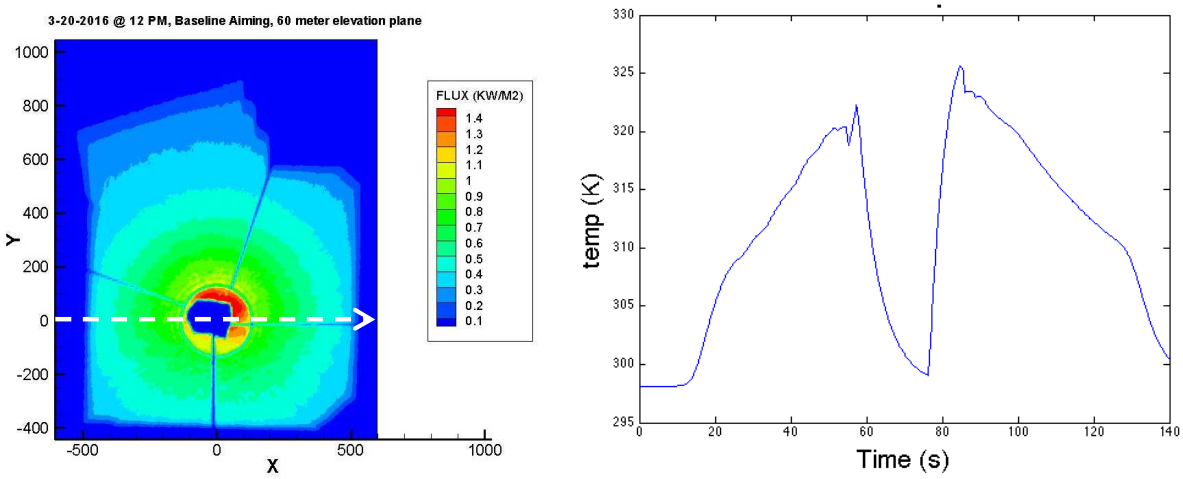

FIGURE 7. Left: Simulated irradiance at Ivanpah Unit 2 along a horizontal plane 60 m above the ground for the baseline heliostat standby aiming strategy. Right: Simulated bird feather temperature during flight along dashed transect in left image using baseline parameter values.

CONCLUSIONS

A heat-transfer and solar-flux model has been developed to determine the feather temperature along prescribed bird flight paths with varying solar irradiances. Probabilistic modeling results show that the irradiance and assumed feather properties (thickness, absorptance, heat capacity) have the most significant impact on the simulated feather temperature, which can increase rapidly depending on the parameter values. The avian flux hazard model is being combined with a plant performance model to identify alternative heliostat standby aiming strategies that minimize both avian flux hazards and negative impacts on plant performance.

ACKNOWLEDGMENTS

The authors thank Doug Davis of NRG, who provided information on the Ivanpah heliostat field and avian mortality studies. Sandia National Laboratories is a multi-program laboratory managed and operated by Sandia Corporation, a wholly owned subsidiary of Lockheed Martin Corporation, for the U.S. Department of Energy's National Nuclear Security Administration under contract DE-AC04-94AL85000.

REFERENCES

1. H. T. Harvey and Associates, Ivanpah Solar Electric Generating System Avian & Bat Monitoring Plan - 2013-2014 Annual Report (Revised), Docket Number 07-AFC-05C, TN#204258, 2015, Available from: https://efiling.energy.ca.gov/Lists/DocketLog.aspx?docketnumber=07-AFC-05C.
2. C. K. Ho, Review of Avian Mortality Studies at Concentrating Solar Power Plants, in SolarPACES 2015, Cape Town, South Africa, October 13 - 16, 2015.
3. R. A. Kagan, T. C. Viner, P. W. Trail and E. O. Espinoza, Avian Mortality at Solar Energy Facilities in Southern California: A Preliminary Analysis, 2014.
4. L.J. Walston et al., A Review of Avian Monitoring and Mitigation Information at Existing Utility-Scale Solar Facilities, Report No. ANL/EVS-15/2, 2015.
5. M. D. Mccrary, R. L. Mckernan, R. W. Schreiber, W. D. Wagner and T. C. Sciarrotta, Avian Mortality at a Solar-Energy Power-Plant, J Field Ornithol 57 (2), 135-141 (1986).
6. I. Western EcoSystems Technology, Ivanpah Solar Electric Generating System Avian & Bat Monitoring Plan - 2014-2015 Annual Report and Two-Year Comparison 21 October 2014 – 20 October 2015, Docket Number 07-AFC-05C, TN#212042, 2016, Available from: https://efiling.energy.ca.gov/Lists/DocketLog.aspx?docketnumber=07-AFC-05C.
7. S. Kraemer. One Weird trick Prevents Bird Deaths at Solar Towers. 2015 April 16, 2015; Available from: http://cleantechnica.com/2015/04/16/one-weird-trick-prevents-bird-deaths-solar-towers/.
8. J. Vittori, Information Request - 2015 Avian Mortality Tracking, Memorandum to Tonopah Solar Energy, LLC, Memorandum to Mary Grikas - Tonopah Solar Energy, LLC, 2015.
9. National Renewable Energy Laboratory. System Advisor Model. 2012; Available from: https://sam.nrel.gov/.
10. E. Senoz, R. P. Wool, C. W. J. McChalicher and C. K. Hong, Physical and chemical changes in feather keratin during pyrolysis, Polym Degrad Stabil 97 (3), 297-307 (2012).
11. K. Takahashi, H. Yamamoto, Y. Yokote and M. Hattori, Thermal behavior of fowl feather keratin, Biosci Biotech Bioch 68 (9), 1875-1881 (2004).
12. California Energy Commission (Tyler et al.), Appendix BIO1 - Biologocial Resources Risk Assessment of Avian Exposure to Concentrated Solar Radiation, Final Staff Assessment for the Hidden Hills Solar Electric Generating System Project, 2012.
13. T. A. Harvey, K. S. Bostwick and S. Marschner, Directional reflectance and milli-scale feather morphology of the African Emerald Cuckoo, Chrysococcyx cupreus, J R Soc Interface 10 (86) (2013).
14. F. P. Incropera, D.P. DeWitt, Introduction to Heat Transfer. (John Wiley & Sons, New York, 1985).
15. D. Yildiz, E. U. Bozkurt and S. H. Akturks, Determination of Goose Feather Morphology by Using SEM, J Anim Vet Adv 8 (12), 2650-2654 (2009).
16. B. O. Wolf and G. E. Walsberg, The role of the plumage in heat transfer processes of birds, Am Zool 40 (4), 575-584 (2000).
17. G. E. Walsberg, Heat-Flow through Avian Plumages - the Relative Importance of Conduction, Convection, and Radiation, J Therm Biol 13 (2), 89-92 (1988).
18. M. J. Wagner, SolarPILOT User's Manual: A Tool for Solar Power Tower Layout and Optimization, 2015.